Available online at www.sciencedirect.com

ScienceDirect

journal homepage: www.elsevier.com/locate/nanoenergy

FULL PAPER

Dispersion of carbon nanotubes in aluminum improves radiation resistance

Kang Pyo So[a], Di Chen[b], Akihiro Kushima[a], Mingda Li[a],
Sangtae Kim[a], Yang Yang[a], Ziqiang Wang[a], Jong Gil Park[c],
Young Hee Lee[c], Rafael I. Gonzalez[d], Miguel Kiwi[d],
Eduardo M. Bringa[e], Lin Shao[b,*], Ju Li[a,*]

[a]Department of Nuclear Science and Engineering and Department of Materials Science and Engineering, Massachusetts Institute of Technology, Cambridge, MA 02139, USA
[b]Department of Nuclear Engineering, Texas A&M University, College Station, TX 77845, USA
[c]IBS Center for Integrated Nanostructure Physics, Institute for Basic Science (IBS), Sungkyunkwan University, 440-746, Republic of Korea
[d]Departamento de Fisica, Facultad de Ciencias, Universidad de Chile, Casilla 653, Santiago 7800024, Chile
[e]Facultad de Ciencias Exactas y Naturales, Universidad Nacional de Cuyo, Mendoza 5500, Argentina

Abstract
We can mass-produce metal/carbon nanotube (CNT) composites that show improved radiation tolerance. The 0.5 wt% Al+CNT composite showed improved tensile strength without reduction of tensile ductility before radiation, and reduced void/pore generation and radiation embrittlement at high displacements per atom (DPA). Under helium ion irradiation up to 72 DPA, the 1D carbon nanostructures survive, while sp^2 bonded graphene transforms to sp^3 tetrahedral amorphous carbon. Self-ion (Al) irradiation converts CNTs to a metastable form of Al_4C_3, but still as slender 1D nanorods with prolific internal interfaces that catalyze recombination of radiation defects, reducing radiation hardening and porosity generation. The 1D fillers may also form percolating paths of "nano-chimneys" that outgas the accumulated helium and other fission gases, providing an essential solution to the gas accumulation problem.
© 2016 Elsevier Ltd. All rights reserved.

Nuclear fission and fusion reactors, nuclear waste containment, nuclear batteries and space explorations demand materials with extraordinary thermomechanical properties and radiation resistance. Radiation can induce severe

*Corresponding authors.
 E-mail addresses: lshao@tamu.edu (L. Shao), liju@mit.edu (J. Li).

damages in materials, including swelling, hardening, creep, embrittlement and irradiation-assisted corrosion [1,2]. The tolerance of radiation damage by structural materials plays a significant role in the safety and economy of nuclear energy [2], as well as the lifetime of nuclear batteries, spaceships and nuclear waste containers, as they are often exposed to long-term radiation [3,4].

Nanostructuring is a key strategy to improve the radiation resistance of materials [5-8]. Carbon nanotubes (CNTs) are well known to be a strong and flexible nanomaterial. If CNTs are uniformly dispersed inside metal as 1D fillers [9-11], its high aspect ratio η (up to 10^8) [12] should create prolific internal interfaces with the metal matrix that may act as venues for the radiation defects to recombine (self-heal). In addition, based on percolation theory and geometrical simulations [13,14], a random 3D network of 1D fillers can form globally percolating transport paths even with diminishing volume fraction $\phi \to 0$, if $\eta \to \infty$. 1D fillers can be efficient for this purpose, considering for example cardiovascular and plant root systems that are 1D transport networks. Helium (alpha particle) accumulation inside materials [15] is a known problem that exacerbates embrittlement and swelling [16]. If the 1D fillers form globally percolating paths of "nano-chimneys" that can outgas the accumulated helium [17] and other fission gases to an external fission-product gettering/trapping system [18], they might provide an essential solution to the problem.

Key questions regarding metal-CNT composite (MCC) in the nuclear environment are:

(i) Does the dispersion of CNTs degrade thermomechanical properties (strength, toughness, thermal conductivity [19], etc.) before irradiation?

(ii) Once radiation starts, is radiation embrittlement and swelling reduced (due to self-healing effect of the filler-metal interfaces) in MCC compared to the control metal?

(iii) Even if 1D nano-fillers improve (i) and (ii), how stable are these 1D nano-fillers themselves under heavy dose of radiation? Typical radiation exposure to the nuclear fuel cladding material is ~ 15 DPA (displacements per atom) before they are taken out of the reactor. Core internals in commercial light-water reactors should sustain around 80 DPA after 40 years of plant operations [20], and advanced fast reactors would demand even more.

In this paper we investigate the basic radiation materials science of MCC, in particular Al+CNT composite, using a high-energy ion accelerator to inject He and Al ions which generate atomic displacements in the composite, in lieu of neutrons. We find that in addition to property improvements (i) and (ii), the 1D form factor of nano-fillers does survive up to 72 DPA of He ion irradiation, and also 72 DPA of Al self-ion radiation at room temperature, which is intriguing because every carbon and aluminum atoms are knocked out $\sim 10^2$ times, yet the 1D nano-morphologies survive, along with the prolific internal interfaces. The morphological robustness of 1D nano-fillers in non-equilibrium conditions is reminiscent of nanowire growth in chemical vapor deposition that violates equilibrium Wulff construction, and the presence of CNTs in ancient Damascus steel [21] (as the equilibrium

phase diagram would indicate that CNTs should be converted to blocky graphite).

We have synthesized Al+CNT composites, as aluminum is cheap and very widely used. Al can be used as the fuel cladding materials in research reactors, as well as containment for nuclear waste, components for robots in radiation environments, etc. Its light density may impart significant advantage for space applications. Al has low thermal neutron absorption cross-section of 0.232 barn, above only those of Mg (0.063 barn), Pb (0.171 barn) and Zr (0.184 barn) among structural metals, and high corrosion resistance in water, therefore it is already widely used in low-temperature research reactors [22]. The development of Al+CNT may not only benefit research reactors, but also provide guidance for designing new kinds of cladding materials (e.g., Zr+CNT, Stainless-steel+CNT) that can be used in commercial reactors. Second, Al is used in nuclear battery since it is reflective, and has low production rate of Bremsstrahlung radiation due to low atomic number. Thus it has been recommended for several components in designs of nuclear battery such as shielding, current collector [23] and electrode [24]. Al+CNT will increase the lifetime of nuclear battery because of better radiation resistance. This composite may also alleviate helium accumulation from alpha decay, which is one of the main engineering issues associated with radioisotope thermoelectric generator (RTG) [4].

We have performed accelerator-based ion irradiation tests on Al+CNT (and pure Al control) at room temperature (homologous temperature $T/T_M = 0.32$, Al's melting point is $T_M = 933.47$ K). At this range, volumetric swelling from void formation becomes prominent when radiation exposure is larger than 10 DPA [2].

Modification of interfaces of 1D nanostructure upon irradiation plays an essential role for MCC properties. Figure 1 provides a schematic illustration of ion beam interaction with CNT. The energies of incoming ions are absorbed and transform CNT structure to rearranged carbon nanostructure, or aluminum carbide nanorods, depending on the ion type and beam energy. The 1D interfaces, if they survive, likely reduce the supersaturation of radiation-generated vacancies, by boosting recombination with self-interstitial atoms (SIA) and interstitial clusters. The light-weight ion irradiation generally generates more "sparse" collision cascades with lower defect density and shorter length compared to heavy ions. Therefore, He ion irradiation causes less Al/C mixing than Al ion irradiation since an interstitial Al atom can quickly find the nearest vacancy of the same chemical species. The CNT undergoes restructuring, making a helical carbon nanostructure, as shown in Figure 1 with a yellow arrow. Irradiation with heavier Al ions, which produces "denser" collision cascades and more Al/C mixing [25], eventually changes the composition of CNT fillers, forming an aluminum carbide phase with 1D nanorod morphology (blue arrow).

For (i), (ii), fabrication of high-quality and low-porosity composite is essential. Achieving uniform CNTs dispersion without inducing degradation to CNTs or Al matrix is the key here. Our specimen preparation consists of three steps (Figure 2A): (step i) declustering of the CNTs on the surface of Al particles, (step ii) encapsulation of the dispersed CNTs and further consolidation into Al particles to form Al-C

Figure 1 Schematic illustration of shape changes on CNT, recombination, and helium out-gas. Under ion irradiation, the disintegration of CNT and formation of aluminum carbide (blue arrow) from high energy ion and restructuring to helical CNT structure (yellow arrow) from low energy ion are indicated.
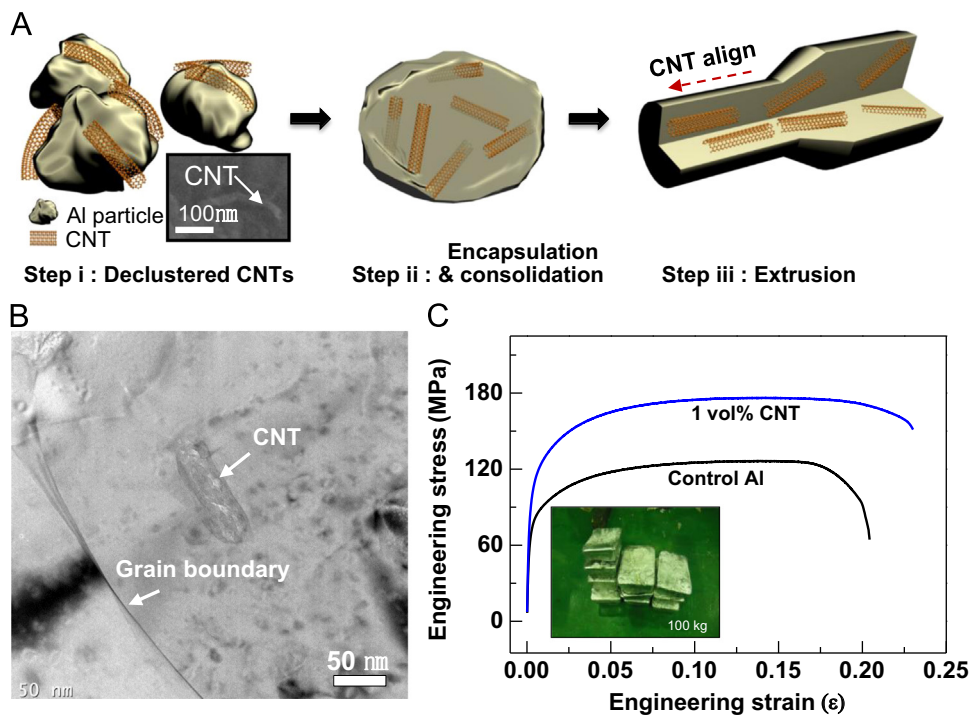
Figure 2 Fabrication process and microstructure/mechanical properties of Al+CNT composites. (A) A schematic representation for the fabrication of Al+CNT composite. (B) Dispersion of CNT inside Al grain in TEM, (C) Stress-strain curve (inset: 100 kg of the Al +CNT composite). Dispersion of CNTs in grain improves the tensile strength without sacrificing ductility.

covalent bonds by spark plasma sintering (SPS), and (step iii) hot extrusion. We used multi-walled carbon nanotubes (MWCNTs) with 10-30 nm in the diameter D and 10 μm in the length L ($\eta \equiv L/D = 300$-1000). The optimized processing conditions are described in detail in Supplementary Online Materials (SOM). This process is industrially scalable, and we have already produced Al+CNT nanocomposite weighing more than 100 kg, as shown in Figure 2C (inset). Cost analysis indicates that its specific weight cost (including raw material cost of MWCNTs and processing costs) should be less than two times the price of bulk-scale Al alloy. The

G-mode mapping from confocal Raman indicate the dispersion of CNTs in Figure S1 A and B. Transmission electron microscopy (TEM) observation further verified that CNT embedded inside the Al grain as indicated by the white arrow in Figure 2B. These observations are the evidence that CNTs were highly dispersed after the processing. A bulk specimen for ASTM E8 standard tensile testing, fabricated after hot extrusion, is used for mechanical properties testing. Typical stress-strain curves for the samples with different MWCNTs volume fraction ϕ are shown in Figure 2C. The tensile strength was enhanced by 34% at 1 vol% MWCNTs
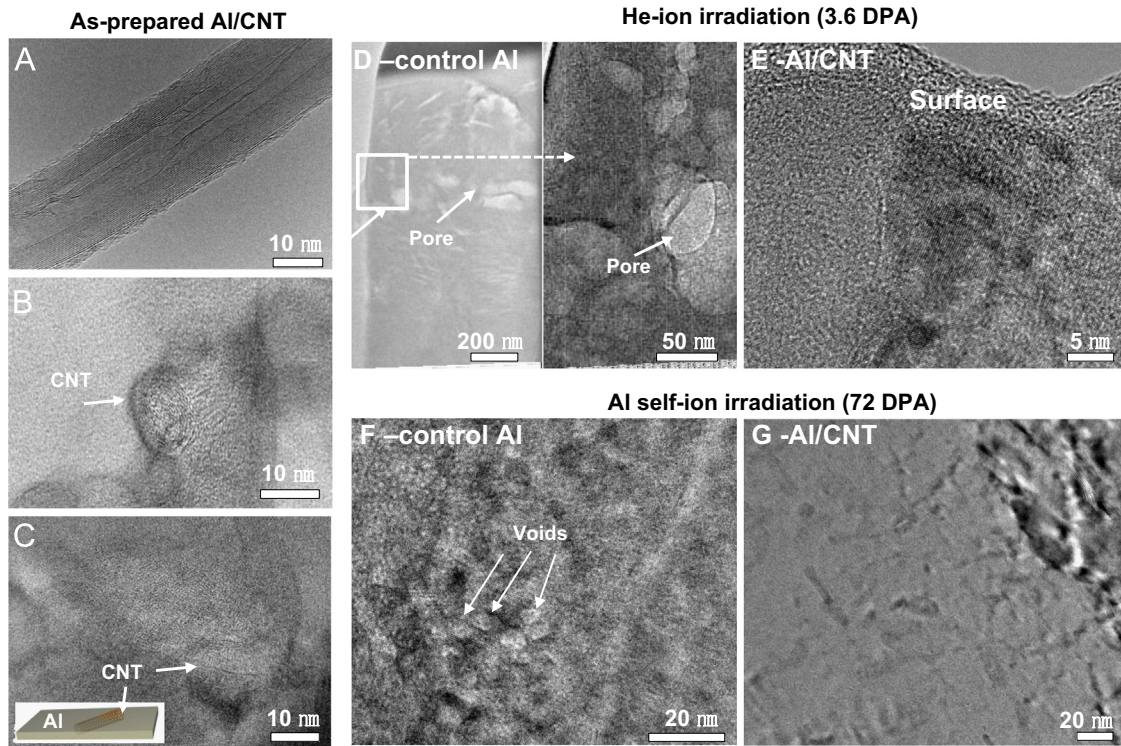
Figure 3 Structural evolution of Al+CNT composite under ion irradiation. TEM image of (A) pristine CNT, (B) and (C) intact wall structure of CNT in Al matrix. Microstructure of (D) control Al and (E) Al+CNT after helium ion irradiation at 3.6 DPA, (F) control Al and (G) Al+CNT after aluminum self-ion irradiation at 72 DPA. Note, no pores were generated by dispersing the 1 vol% of CNT in Al matrix in (E) and (G).

(ϕ=0.01), without sacrificing tensile ductility. As shown in Figure S1C, MWCNTs strands are seen to be protruding out of the fractured area, as indicated by the white arrows. This fiber pull-out between CNTs and Al induces load transfer and improves fracture toughness [26].

To test the radiation tolerance of the Al+CNT composite, the sample was irradiated by 100 keV helium ions and 2 MeV aluminum self-ion up to 3.6, 16 and 72 DPA (see SOM), respectively. The results were compared with the pure Al control samples under the same irradiation conditions. The diameter of the inner space and the wall thickness of the MWCNT are 10 nm and 7–10 nm, respectively, as indicated in the TEM image in Figure 3A. The initial geometry does resemble a "nano-chimney". The graphene walls of the CNTs were clearly visible in the TEM images shown in Figure 3B and C, indicating no significant chemical mixing the CNTs. If the MWCNTs are entirely straight and randomly distributed, then analytical modeling and Monte Carlo simulations gives percolation threshold estimate [13,14]:

$$\phi_c \approx \frac{1}{2\frac{L}{D}+3+\pi+\frac{\pi}{2}\frac{D}{L}} \tag{1}$$

which for aspect ratio $\eta \equiv L/D = 300$, gives $\phi_c = 0.0016$, and for $\eta \equiv L/D = 1000$, gives $\phi_c = 5 \times 10^{-4}$. The MWCNT volume fraction we have here is an order of magnitude larger than ϕ_c, therefore the MWCNTs should form a globally percolating network of nano-chimneys. Helium gas is expected to travel facilely in 1D hollow structures like MWCNTs with smooth interior walls.[17]

Figures 3D and E show the control Al samples after 3.6 DPA He-ion irradiation and 72 DPA Al self-ion irradiation,

respectively. The irradiation generates nanocavities inside by the aggregation of radiation-induced vacancies, and the positive He gas pressure further stabilizes the bigger cavities compared to Al-ion irradiation. Bubbles appear at just 3.6 DPA in pure Al for He-ion irradiation. The formation of large cavities with diameters ranging 100–200 nm was observed in the control Al (Figure 3D left). The higher magnification indicates that small cavities were also generated (Figure 3D right). In contrast, the Al+CNT 1 vol% sample has no cavity generation at the same DPA (Figure 3E). The higher magnification provides clear evidence of no bubble/void generation at 3.6 DPA He-ion irradiation (Figure 3F) in Al+CNT. Furthermore, no cavity was observed even after 72 DPA Al self-ion irradiation of the Al+CNT (Figure 3G). CNTs dispersed inside Al grain seem to suppress cavity generation completely up to at least 3.6 DPA for He-ion and 72 DPA for Al self-ion radiation, and the answer to (ii) should be positive from the structural point of view.

He-ion radiation to 72 DPA was further carried out to study severe radiation damage condition. Large cavities about 500 nm in diameter were observed in Al without CNTs (Figures 4A and S3A). The surface indicates obvious surface cracking occurred from the volume expansion of the cavities after the irradiation (Figure S2A, bottom). Cavities are also generated in Al+CNT 1 vol% sample at 72 DPA He-ion irradiation, but much smaller than those of control Al (Figures 4B and S3B). The largest cavity is 170 nm in diameter, 20 times smaller in volume than the pore in the control Al. This suggests that the incorporation of MWCNTs in Al suppresses porosity development in severe radiation
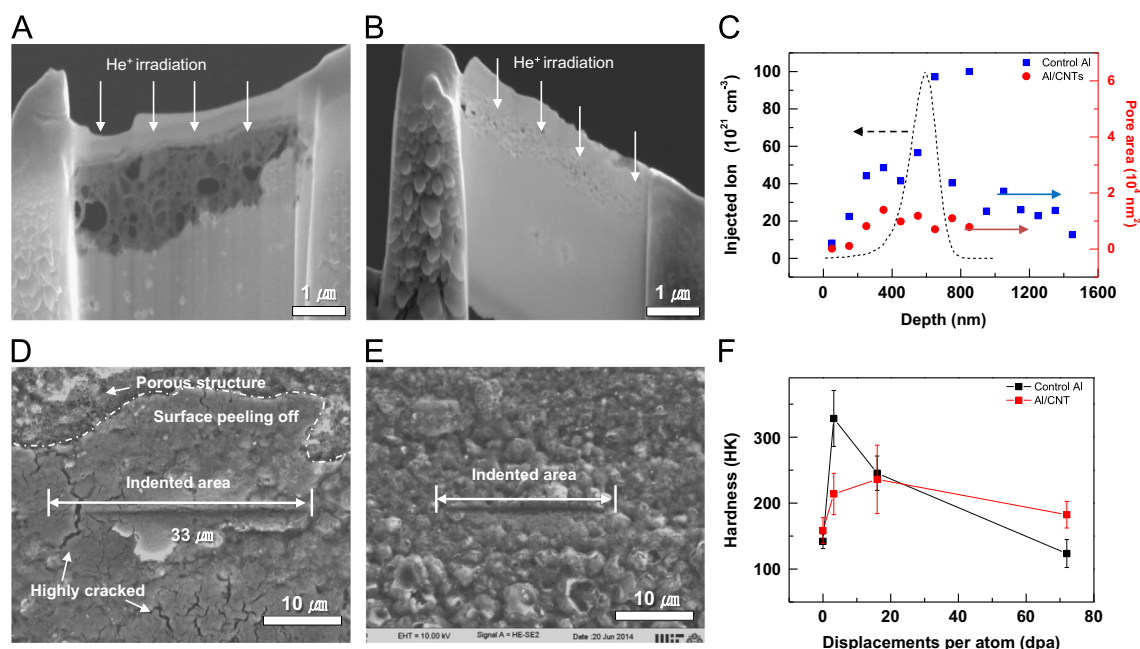
Figure 4 Quantification and mechanical responses of pore generation after 72 DPA helium ion irradiation. SEM image of (A) highly porous control Al and (B) Al+CNT 1 vol%. (C) Injected ion (SRIM) and pore areas versus depth, for 100 keV He ion injection to 72 DPA peak damage. Indented area observation on (D) control Al and (E) Al+CNT composites. Note, highly cracked and porous structure are observed near indented areas in control Al. (F) Knoop hardness versus DPA.

damage conditions. This obvious reduction of porosity in Al-CNTs composite implies that He gas diffused out of Al matrix robustly. Two mechanisms are possible: i) He gas diffused out along the CNT-metal interface, or ii) the interspace and central hollow space inside CNTs acts as 'nano-chimneys' for diffusion of He gas. Since the mechanical strength is enhanced significantly by load transfer associated with strong anchoring of Al onto the CNT surface [9,27], the possibility of the former is small. Therefore, we believe that the globally percolating "nano-chimney" network plays a role for He outgassing.

To quantify the effect of carbon on the radiation damage induced by He ion irradiation in the Al, the stopping and range of ions in matter (SRIM-2013) simulation [srim.org] was performed with/without carbon element in the Al matrix. The carbon content of Al+1 vol% CNT was roughly 0.5 wt%. In the simulation, we uniformly dispersed carbon atoms in the Al matrix to extract the effect of the carbon atoms alone. The maximum DPA is predicted to occur at 534 nm in depth, slightly shallower than the maximum peak (596 nm) of injected He ion. Exactly the same DPA profiles were observed regardless of the presence of carbon, as shown in Figure S4. The 0.5 wt% carbon in Al hence has negligible influence on the helium injection and DPA profiles. Figure 3C shows the relationship between the injected ion/pore generations versus the depth. The simulated damage profiles agree well with the experimentally observed porosity generation profile. However, the absolute cavity area and the size are significantly smaller in the Al+CNT composites than in the control sample. This suggests that the MWCNTs giving high internal interface area is key to

the reduced porosity creation. More detailed modeling including the shapes of the MWCNT inclusion and the CNT-Al interactions is necessary to precisely quantify the structural effect, which is beyond the scope of this paper.

If the MWCNTs are randomly dispersed, then the furthest distance between any point of its nearest MWCNTs scales as $L_{furthest} \propto D\phi^{-1/2}$ (D=diameter). For our 1 vol% MWCNT sample, $L_{furthest}$ should be around 200 nm. This is still an order of magnitude longer than the typical size of a radiation cascade, which is 10-20 nm, therefore the improvement in porosity suggests that porosity development involves length scales quite beyond a single cascade annealing. For comparison, ultra-fine grained austenitic stainless steel with a grain size of 100 nm was recently shown to exhibit 5 times slower void swelling rate up to 80 DPA [7], and $L_{furthest}$ in that case should be around 50 nm if all the grain boundaries (GB) are effective venues for recombination. Compared to that system of "2D nanoengineered" network of GBs [7], our "1D nanoengineered" CNTs/Al has 4 times longer $L_{furthest}$ and 15 times less interfacial area per volume. Yet our system seems to be still similarly effective in cavity suppression.

The above demonstrates aplenty that Al+CNT composite was successful in reducing the structural damage. To show that it leads to property improvement, we conducted micro hardness test to evaluate the change in strength of Al+CNT under radiation exposure. Since the irradiation damage from the ion accelerator was localized beneath the surface within 1 μm depth, we selected the Knoop micro-hardness test to quantify the mechanical behavior in the damaged region. The Knoop micro-hardness test is specially designed

for thin film samples. Cracks and porous structure under the surface were observed in the control Al after the Knoop indentation, whereas Al+CNT sample showed almost no cracks, as seen in Figures 4D and E, indicating that the Al +CNT sample has less irradiation embrittlement and swelling. The hardness value further verify this observation. The hardness change was measured as a function of DPA as shown in Figure 4F. Note that the hardness increased up to 328 HK at 3.6 DPA in the control Al. In contrast, our Al+CNT nanocomposite, even though it starts out having higher hardness by virtue of higher strength (i), hardens much less compared to control Al (ii). The initial radiation hardening observed in metallic materials results from the obstacles to dislocations, such as point-defect clusters, stacking fault tetrahedra and cavities, generated by radiation. Thus, we again verifies that our "1D nanoengineered" Al+CNT has better radiation tolerance (specifically radiation hardening and embrittlement) compared to the reference control Al.

However, once above 3.6 DPA, the Knoop hardness of control Al decreased with increasing helium ion irradiation dose. This phenomenon could be explained by the severe porosity development which reduced the apparent density of materials. The cavity volume fraction in control Al reached 25% at 72 DPA (Figure 4A). The increasing volume of pores cause the transition from hardening to softening [28], and will result in exceptionally poor toughness as tensile fracture is very sensitive to the size of the largest flaw. In contrast, the cavity volume fraction reached only

4.7% for Al+CNT at 72 DPA, with the largest pore 20 times smaller in volume (Figure S3A and B). Also, the maximum value of the hardness in Al+CNT was reached at 16 DPA (5 times larger dose than control Al), and the 240 HK peak hardening value was much lower than that of the control Al. We are thus confident that the mechanical properties of Al +CNT is more tolerant of both low and high doses of radiation.

High-resolution TEM (HRTEM) was performed on the post-irradiated Al+CNT, as shown in Figure 5A and B. Several tubular cross-sectional structures near each pore were observed (Figure 5A). The tubular structure is still retained after 72 DPA He-ion radiation. Some of the tubular walls merged with each other and the helical shapes were also found, as shown in Figure 1 [29]. Thus, the 1D nano-fillers maintain its general tubular morphology under the He ion irradiation (which generates sparser cascades). Raman spectroscopy indicates quite drastic changes in atomic bonding inside the tubules at higher DPA He-ion irradiation, as confirmed from Raman spectra of D and G bands in Figure 5C. The strong signal near 1440 cm^{-1} corresponds to tetrahedral amorphous carbon (ta–C) with highest sp^3 content (80–90%) [30]. Electron energy loss spectroscopy (EELS) mapping in TEM shows the region with a high carbon concentration (20 nm in width) corresponding to the original diameter of the CNT (Figures 3A and S6B). The sp^3/sp^2 mapping results (Figure S6C and D) indicate strong sp^3 signal at the region of high carbon concentration (see SOM
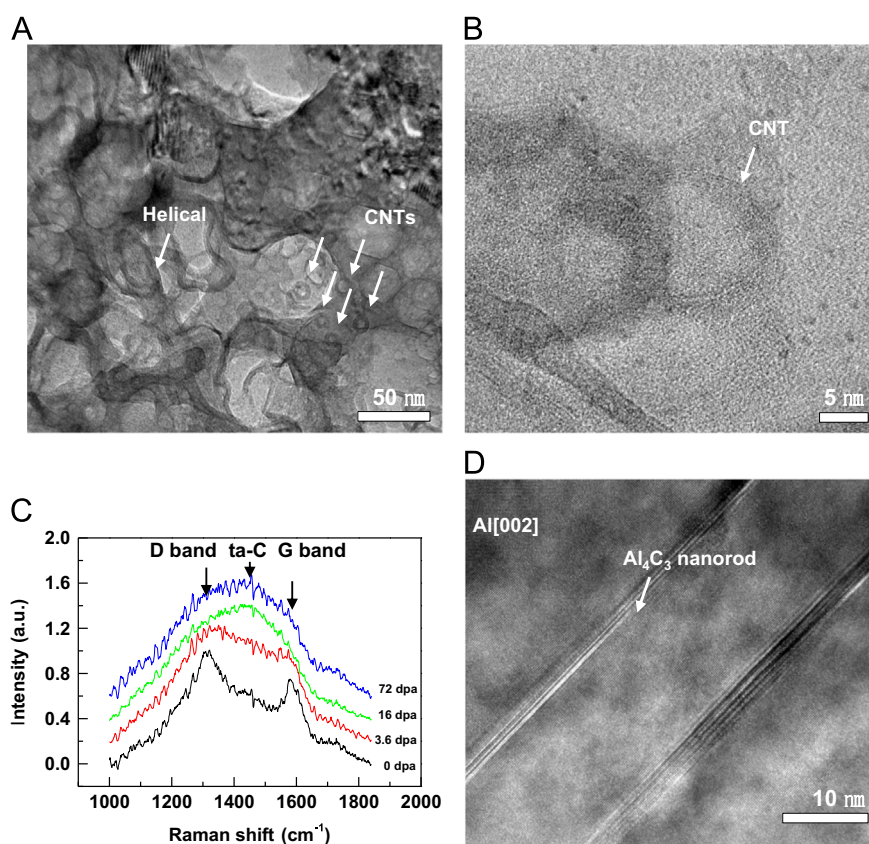
Figure 5 Structure of CNT after 72 DPA irradiation. (A) Traces and (B) wall structure of CNTs after helium ion irradiation, and (C) Raman spectrum at different DPA. (D) Al$_4$C$_3$ nanocarbide under 72 DPA Al self-ion irradiation. *Note:* the structure of Al$_4$C$_3$ nanocarbide is described in supplementary (Figure S8).

for detail). The observations suggest that the carbon tubular nanostructures observed in TEM are composed of diamond-like carbon with tetrahedral amorphous sp^3 bonding, instead of aluminum carbide (Al_4C_3) which should form according to the equilibrium phase diagram below $2160\,°C$ [31].

In reference to pure Al and graphite, the Gibbs free energy of formation for the stable phase of Al_4C_3 (rhombohedral) is $-194.4\,kJ/mol$ at room temperature [31] or $-2.01\,eV$ per Al_4C_3 formula unit. On a per carbon basis, it is not as high as ZrC ($-2.14\,eV$ per ZrC [32]), but is comparable to SiC ($-0.76\,eV$ per SiC) and much higher than cementite ($-0.18\,eV$ per Fe_3C). So the fact that much of the carbon nanostructures survive without forming the carbide after 72 DPA He-ion irradiation is somewhat surprising. On the other hand, the conversion of sp^2 bonding of carbon in CNTs to sp^3 of ta-C agrees with the previous understanding of radiation damage of carbon [33].

Aluminum self-ion irradiation with higher energy of 2 MeV ($20\times$ that of helium ion) which creates denser cascades [25] eventually disintegrates the pure carbon nanostructure, and generates slender Al_4C_3 nanocarbides, as shown in Figures 5D and S8, and illustrated in Figure 1. The denser cascade provides higher probability to mix carbon with the matrix aluminum atoms. The 1D nature of Al_4C_3 nanocarbides was confirmed in a series of tilting images inside the TEM. The electron diffraction along Al [001] zone axis on the nanocarbide shows that the new structure embedded in the matrix is not the rhombohedral phase of Al_4C_3 (ICSD number 14397), but a metastable triclinic phase (materialsproject.org mp632442). Density functional theory calculations reveal that, intriguingly, this metastable Al_4C_3 nanocarbide has higher formation energy of about 2.8 eV per formula unit above the rhombohedral phase ground state. This energetic metastability is about 1.877 MJ/kg, almost half of the detonation energy density of TNT. We have also determined that many distinct lattice orientation relationships are present between the newly formed Al_4C_3 and Al matrix, with semicoherent and incoherent interfaces based on high-resolution TEM observations. The 1D nanocarbides likely benefit energetically from the interfacial energy considerations with the matrix, which otherwise would be considered high energy in bulk form. Figure 5D is quite remarkable in that it shows two Al_4C_3 nanocarbides running parallel to each other, separated by ~20 nm, on the order of D of the original MWCNTs. We surmise these two nanocarbides are decomposition products from the same MWCNT, that originally ran in the same direction, like "fly in amber". The high-energy self-ion radiation destroyed the hollowness of the MWCNT and backfilled it with Al, but vestiges of the original 1D nanostructures remain like fossil record. The nanocarbides are thus templated by the original carbon nanostructures, and this *in situ* formation could be a new paradigm for creating radiation-tolerant nanodispersion-strengthened metals.

In summary, we can mass-produce Al-CNT nanocomposite cheaply, at 100 kg scale and at no more than $2\times$ the cost. With regard to question (i), CNTs improve strength while maintaining tensile ductility. Our helium and aluminum ion irradiation experiments demonstrate that uniform dispersion of CNT reduces radiation hardening and embrittlement. These evidences indicate that the answer to (ii) is affirmative, due

to efficient defect recombination at the incoherent CNT-metal interfaces. Detailed microstructural characterizations further demonstrate that the prolific 1D slender form factors are surprisingly robust under radiation, and survive up to 72 DPA of He-ion and Al-ion irradiations, answering question (iii). Therefore, Al–CNT nanocomposite satisfies all three main concerns (i), (ii) and (iii), providing a nanocomposite paradigm to improve components in nuclear fission and fusion reactors, nuclear waste containment, nuclear batteries and space explorations that demand materials with extraordinary thermomechanical properties and radiation resistance.

Acknowledgment

Appendix A. Supplementary material

Supplementary data associated with this article can be found in the online version at http://dx.doi.org/10.1016/j.nanoen.2016.01.019.

References

[1] E.M. Bringa, et al., Nano Lett. 12 (2012) 3351–3355. http://dx.doi.org/10.1021/nl201383u.
[2] S.J. Zinkle, J.T. Busby, Mater. Today 12 (2009) 12–19.
[3] L.S. Novikov, et al., J. Surf. Investig. – X-Ray 3 (2009) 199–214. http://dx.doi.org/10.1134/S1027451009020062.
[4] T. Wacharasindhu, J.W. Kwon, D.E. Meier, J.D. Robertson, Appl. Phys. Lett. 95 (2009) 014103. http://dx.doi.org/10.1063/1.3160542.
[5] I.J. Beyerlein, et al., Mater. Today 16 (2013) 443–449. http://dx.doi.org/10.1016/j.mattod.2013.10.019.
[6] S. Wurster, R. Pippan, Scr. Mater. 60 (2009) 1083–1087. http://dx.doi.org/10.1016/j.scriptamat.2009.01.011.
[7] C. Sun, et al., Sci. Rep. 5 (2015) 7801. http://dx.doi.org/10.1038/srep07801 http://www.nature.com/srep/2015/150115/srep07801/abs/srep07801.html#supplementary-information.
[8] G.R. Odette, JOM 66 (2014) 2427–2441. http://dx.doi.org/10.1007/s11837-014-1207-5.
[9] K.P. So, et al., Acta Mater. 59 (2011) 3313–3320. http://dx.doi.org/10.1016/j.actamat.2011.01.061.
[10] K.P. So, et al., Compos. Sci. Technol. 74 (2013) 6–13. http://dx.doi.org/10.1016/j.compscitech.2012.09.014.
[11] S.R. Bakshi, D. Lahiri, A. Agarwal, Int. Mater. Rev. 55 (2010) 41–64. http://dx.doi.org/10.1179/095066009X12572530170543.

[12] X. Wang, et al., Nano Lett. 9 (2009) 3137–3141. http://dx.doi.org/10.1021/nl901260b.

[13] S.I. White, et al., Adv. Funct. Mater. 20 (2010) 2709–2716. http://dx.doi.org/10.1002/adfm.201000451.

[14] R.M. Mutiso, M.C. Sherrott, J. Li, K.I. Winey, Phys. Rev. B 86 (2012) 214306 87, doi:Artn 019902 1103/Physrevb.87.019902 (2013).

[15] A. Kashinath, A. Misra, M.J. Demkowicz, Phys. Rev. Lett. 110 (2013) 086101.

[16] G.R. Odette, M.J. Alinger, B.D. Wirth, Annu. Rev. Mater. Res. 38 (2008) 471–503. http://dx.doi.org/10.1146/annurev.matsci.38.060407.130315.

[17] H. Verweij, M.C. Schillo, J. Li, Small 3 (2007) 1996–2004. http://dx.doi.org/10.1002/smll.200700368.

[18] A. Schwartz, et al., Postirradiation Examination of Peach Bottom Fuel Elements E05-05 and C05-05 and Related Analyses, Gulf General Atomic, U. S. Atomic Energy Commission, 1969.

[19] J. Li, L. Porter, S. Yip, J. Nucl. Mater. 255 (1998) 139–152. http://dx.doi.org/10.1016/s0022-3115(98)00034-8.

[20] S.J. Zinkle, G.S. Was, Acta Mater. 61 (2013) 735–758. http://dx.doi.org/10.1016/j.actamat.2012.11.004.

[21] M. Reibold, et al., Nature (2006)286 ⟨http://www.nature.com/nature/journal/v444/n7117/suppinfo/444286a_S1.html⟩.

[22] K. Farrell, Mater. Perform. Corros./Waste Mater. 5 (2012) 143–175.

[23] Google Patents, 1958.

[24 H.R. Shanks, Google Patents, 1998.

[25] Rafael I. Gonzalez, et al., Metal-Nanotube Composites as Radiation Resistant Materials, (to be submitted)(2015).

[26] B. Boesl, D. Lahiri, S. Behdad, A. Agarwal, Carbon 69 (2014) 79–85. http://dx.doi.org/10.1016/j.carbon.2013.11.061.

[27] K.P. So, et al., Prevention of Ductility Reduction in CNT-Reinforced Aluminum via Multi-Step Rupturing Process, 2016.

[28] M.F. Ashby, R.F.M. Medalist, MTA 14 (1983) 1755–1769. http://dx.doi.org/10.1007/bf02645546.

[29] M. Terrones, et al., Phys. Rev. Lett. 89 (2002) 075505.

[30] A.C. Ferrari, J. Robertson, Phil. Trans. R. Soc. Lond. A 362 (2004) 2477–2512. http://dx.doi.org/10.1098/rsta.2004.1452.

[31] C. Qiu, R. Metselaar, J. Alloy. Compd. 216 (1994) 55–60. http://dx.doi.org/10.1016/0925-8388(94)91042-1.

[32] J. Li, D. Liao, S. Yip, R. Najafabadi, L. Ecker, J. Appl. Phys. 93 (2003) 9072–9085. http://dx.doi.org/10.1063/1.1567819.

[33] F. Banhart, Rep. Prog. Phys. 62 (1999) 1181–1221, http://dx.doi.org/10.1088/0034-4885/62/8/201.

Dr. Kang Pyo So is a post-doctoral associate in the Department of Nuclear Science & Engineering at Massachusetts Institute of Technology (MIT). He received his Ph.D. at Sungkyunkwan University in 2012. He was post-doctoral fellow at the Institute of New Paradigm of Energy Science Convergence in SKKU in 2012-2013. He has been working on the development of metal-carbon nanotube (CNT) nanocomposites for mechanically strengthened structural materials. Dr. So has paid attention on the developing of industrially scalable process of Al-CNT composites for several years. He has applied/registered >35 technical patents.

Dr. Di Chen was PhD student at Department of nuclear engineering, Texas A&M University in 2008-2015. His research area is nuclear materials, including cladding materials for nuclear reactor and fuel materials for next generation reactors. Basically, his works are to reveal the interactions between ion and related materials, such as Fe based. Zr based alloy and Uranium. In order to discover the mechanisms behind,

both MD simulations and ion irradiations by acceleration are combined together.

Dr. Akihiro Kushima is a Research Scientist in the Department of Nuclear Science and Engineering at Massachusetts Institute of Technology. His research interest is to understand the fundamental materials properties through combination of in situ electron microscopy and atomistic simulations with particular emphasis on energy storage materials. Dr. Kushima completed his Ph.D. and undergraduate studies in the Department of Engineering Physics and Mechanics at Kyoto University, Japan in 2007. Prior to his current position, he conducted postdoctoral studies at MIT (2007-2010) and University of Pennsylvania (2010-2012).
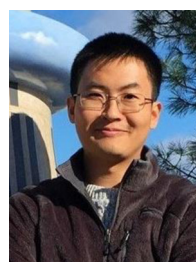
Dr. Mingda Li is currently carrying out his research as a postdoc at Mechanical Engineering Department at MIT, advised by Prof. Gang Chen and Prof. Mildred S. Dresselhaus. In 2015 he received his PhD in Nuclear Science and Engineering Department from MIT, advised by Prof. Ju Li and Dr. Jagadeesh S. Moodera, and previously his BS in Engineering Physics Department from Tsinghua University in 2009, advised by Prof. Ling-An Wu and Prof. Yao Cheng. His research expertise is in radiation applications, including interaction of radiation and matter, nanoscale electron and phonon transport, and neutron, X-ray and electron spectroscopies, etc.

Mr. Sangtae Kim is currently a Ph.D. candidate in Materials Science and Engineering at Massachusetts Institute of Technology, working for Prof. Ju Li. He received a Bachelor of Science in the same field at University of California, Berkeley in 2010. His research interest includes electrochemical system design for energy harvesting, and microstructural engineering via kinetics analysis.
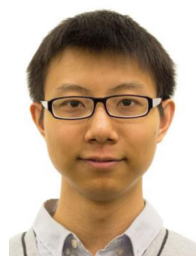
Yang Yang is currently a PhD candidate in Nuclear Science and Engineering of MIT. He focus on nuclear materials and in-situ TEM experiments. He got a Bachelor of Engineering from University of Science and Technology of China in 2008.
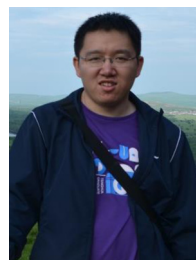
Ziqiang Wang is currently a PhD candidate in Materials Science and Engineering of MIT. He focus on in-situ TEM experiments of lithium ion batteries. He got a Bachelor and Master degree in Tsinghua University.

Jong Gil Park is a Ph.D. candidate in the Center for Integrated Nanostructure Physics (CINAP) at Institute for Basic Science (IBS) and Department of Energy Science at Sung-kyunkwan University (SKKU). He had been working on the industrial development of nanocomposites in the advanced materials research team at Dayou smart aluminum co. ltd.(2008-2013) His research interests are inorganic matrix Nano composites.

Dr. Young Hee Lee is currently a director in the Center for Integrated Nanostructure Physics (CINAP) at Institute for Basic Science (IBS) and a Professor in Department of Energy Science and Department of Physics at Sungkyunkwan University (SKKU). He obtained his Ph.D. in physics from Kent State University in 1986. His research activity has been focused on the new physics phenomena of low dimensional materials with as special emphasis on 2-dimensional layered structures.

Rafael I. González received his Ph.D. in Exact Sciences with mention in Physics from Pontificia Universidad Católica de Chile in 2011. He is currently a postdoctoral researcher at Departament of Physics, Faculty of Sciences, Universidad de Chile and also, he is associated to the Center for the Development of Nanoscience and Nanotechnology (CEDENNA). His research interests include Molecular Dynamics Simulations in Aluminosilicate nanotubes, 2-D materials, nanoparticles and more.

Miguel Kiwi received his Ph.D. at the Univesity of Virginia in 1967. Currently, he is Professor of Physics and Chairman at Department of Physics, Faculty of Sciences, Universidad de Chile. During his career he has published over 130 peer reviewed papers and he has received international recognition. In 2007 he received the Chilean National Science Prize for the Exact Sciences, and in 2013 the Luis Federico Leloir Prize granted by the "Ministerio de Ciencia, Tecnología e Innovación Productiva, República de Argentina", for contributing to foster International Cooperation in Science, Technology and Innovation.

Eduardo M. Bringa received his Ph.D. in Physics at the Univesity of Virginia in 2000. He moved to Lawrence Livermore National Laboratory (LLNL) as a postdoctoral researcher, and he was promoted as staff member in 2003 and permanent staff member in 2007. During 2008 he moved to Mendoza, Argentina, where he is currently a Principal Researcher for CONICET and Full Professor at the School for Natural and Exact Sciences, at the National University of Cuyo (UNCuyo). He is interested in modeling and simulations in general, and collaborates with groups around the world on solving problems in materials science, astrophysics, biology, etc.

Dr. Lin Shao is Associate Professor of Nuclear Engineering at Texas A&M University. He received a BS degree from Peking University and Ph.D from Univ. of Houston, both in Physics. Prior to joining Texas A&M University, he was a Director Funded Postdoctoral Fellow at Los Alamos National Laboratory. His primary research interests are materials degradation under extreme conditions and the development of self-repairing materials for fission reactors. He has published four book chapters, over 160 journal papers and holds 6 US patents. Currently, he is director of the accelerator laboratory at Texas A&M University.

Ju Li is BEA Professor of Nuclear Science and Engineering and Professor of Materials Science and Engineering at MIT. His group (http://Li.mit.edu) performs computational and experimental research on mechanical properties of materials, and energy storage and conversion. Ju is a recipient of the 2005 Presidential Early Career Award for Scientists and Engineers, 2006 MRS Outstanding Young Investigator Award, and 2007 TR35 award from Technology Review magazine. Thomson Reuters included Ju in its Highly Cited Researchers list in 2014, among 147 global scientists in the Materials Science category. Ju was elected Fellow of the American Physical Society in 2014.

SUPPLEMENTARY INFORMATION

Materials and Methods

A. *Experiment*

Sample preparation

The nano-dispersion-assisted declustering (NDaDC) process used for Al/CNT composite fabrication consisted of three steps to incorporate a uniform dispersion of CNT into the Al matrix (Fig. 1A), including (step i) the CNT declustering process on the surface of the Al particles, (step ii) the encapsulation of the dispersed CNT and the further consolidation into Al particles to form Al–C covalent bonds by spark plasma sintering (SPS), and (step iii) extrusion. One gram of multiwalled carbon nanotubes (MWCNT), (CM95, Hanwha Nanotech, Korea) was declustered on 99 g of Al alloy powder (table S1) by means of a high-speed blade mixer (VM0104, Vita-Mix, USA) for 20 min at max. 37,000 rpm. The declustered CNT were encapsulated with additional Al powder using a planetary ball miller (J.E. Powder, Korea) for 30 min at 250 rpm. Encapsulation was necessary to protect the CNT from being severely damaged as a result of mechanical pulverization during further dispersion. For the CNT volume calculation, a CNT density of 1.3 g/cm^3 was used. The process was completed in a glove box (M.O. Tech, Korea) under less than 1 ppm of oxygen and moisture to prevent oxidation. The encapsulated CNT and Al particles were further consolidated under 40 MPa with spark plasma sintering (SPS, 50 t, 50 kW, Eltek, Korea) at 560 °C for 15 min. The bulk Al/CNT composites were extruded to 2.5 mm in diameter with an extrusion ratio of 9:1 at 550 °C.

Ion irradiation

Extruded 2.5 mm of control Al and Al/CNT wire was irradiated at the room temperature. For helium ion irradiation, the total influences of irradiation were 1×10^{17}, 5×10^{17} and 2×10^{18} ions/cm^2 at a constant beam current of 400 nA, 5 uA and 5 uA, respectively, under the 100 keV of acceleration voltage. For aluminium self-ion irradiation, the total influence were 1×10^{17}, 3.75×10^{16} and 1.5×10^{17} ions/cm^2 under the 2 MeV of acceleration voltage. These irradiation conditions are correspond to 3.6, 16 and 72 DPA at maximum point. The experimental parameters are summarized in table S2.

B. SRIM calculation

A random C distribution was assumed for the SRIM estimation, but stopping by MWCNT is complex, and has been recently addressed[1]. Therefore, the geometrical factor of MWCNT has not been considered in this calculation. We assumed a displacement energy of 25 eV in the SRIM2013 calculation (the default displacement energy of 25 eV for Al is the same)[2].

C. VASP simulation

Vienna Ab-initio Simulation Package (VASP) is used to compute the structure of Al_4C_3. Calculations are carried out using generalized gradient approximation (GGA) in the PBE form for the exchange-correlation functional. To ensure convergence, we adopt 520eV plane wave cutoff and 20x20x20 Monkhorst-Pack grid summarized in Table S3.

D. Measurements

The microstructure of the helium ion irradiated samples was characterized by high-resolution SEM (HRSEM, Merlin, ZEISS) and high-resolution TEM (HRTEM, 200 keV, 2010F, JEOL). The TEM sample was prepared using focused ion beam (FIB, Helios Nanolab 6000, FEI) with a Ga ion milling process and a Pt protection layer. The sample was cut from the surface because helium ion penetration depth is less than 1 um. The cavity in all the samples were determined by under/over focusing under TEM. The sizes and cavities were characterized by measuring diameter of all the cavities according to the depth from Fig. S3. The average diameters of cavitis versus

depth were determined by area-weighted average diameter, $d_{av} = \frac{\Sigma_i^n d(i)A(i)}{\Sigma_i^n A(i)}$, affected by contribution from the area of cavities.

The CNT in the Al matrix was characterized using a home-built confocal Raman spectroscopy at 785 nm excitation[3]. (note: Raman spectroscopy (Reinshaw, UK) of reference aluminum carbide (Al_4C_3, 98%, 325 mesh, sigma-aldrich) was measured at 633 nm excitation.) The spectrum of 0 dpa indicate partial aluminum carbide peak near 490, 714 and 860 nm in Fig. S7. The small aluminum carbide is considered to be form during the fabrication process of the Al/CNT composite such as sintering. However, no intensity changes after He ion irradiation whereas G and D band significant shrinks. This phenomenon implies the carbon from CNT transform to diamond-like carbon instead of aluminum carbide.

The surface mechanical properties were characterized by Knoop hardness (hardness, LM 248 AT, LECO, USA) The test was carried out under 10 g force for 10 s, in which a ~30 μm dimple length was created, as indicated in Fig. S5. The depth to dimple length ratio is 1/30, indicating the depth of indentation was ~1 μm.[4]. The dimpled length was used for hardness calculation following equation[4].

$$\mathrm{H}K = 14229 \times P / d^2$$

Where: P is force, gf, and d is length of long diagonal, μm

Scanning transmission electron microscopy (STEM) – high angular annular dark field (HAADF) image indicate that the black area is the cavity or very thin area in the cross section sample as shown in Fig. S6A. The sp^3/sp^2 mapping of was collected from σ* and π* in electron energy loss spectrum (EELS) as shown in Fig S6D. The fingerprint features of carbon on EELS for sp^2 bonding (graphite) and sp^3 bonding (diamond) is that the σ* peak for sp^3 bonding is enhanced significantly while π* peak is reduced significantly, in contrary to that for sp^2 bonding[5]. Quantitatively, we can use the ratio of the integral of an energy box (about 2eV) around σ* peak to that of π* peak, to give out the sp^3/sp^2 bonding mapping for carbon elements[6].

Figure legends:

Fig. S1.| Microscopic dispersion of CNTs using confocal Raman spectroscopy: (A) optical image of Al/CNTs composite after extrusion and (B) G mode mapping from confocal Raman. (C) fractured area at CNT 2 vol%.

Fig. S2.| Surface of samples: (A) Control Al and (B) Al/CNT 1 vol% before (top) and after (bottom) 72 DPA helium ion irradiation.

Fig. S3.| TEM image of the (A) and (B) control Al and (C) and (D) CNT 1 vol% after helium ion irradiation. (A) and (C) are irradiated at 3.6 DPA, and (B) and (D) are irradiated at 72 DPA.

Fig. S4.| The depth profile of radiation damage in unit of (A) displacements per atom (DPA)/ injected helium ion obtained from SRIM simulation and (B) area-weighted average diameter of cavities from TEM. Exactly same profile of injected ion is observed in (A), regardless of 0.5 wt% carbon addition.

Fig. S5.| Indented area of (A) control Al and (B) Al/CNT. Upper image indicated the line shape dimple of the Knoop (top, 10 gf, 16 dpa) and lower image is the rhombus shape dimple of Vickers (bottom, 100 gf, 72 dpa).

Fig. S6.| (A) STEM (HAADF) image; the black area is the cavity or very thin area in the cross section sample. (B) C/Al density ratio temperature mapping, Yellow colour indicate higher

concentration of carbon. (C) The mapping of sp^3/sp^2 ratios of carbon element. (D)EELS spectrum of the carbon in area α from (C).

Fig. S7.| Raman spectrum for comparison of Al_4C_3 and irradiated Al+CNT composite.

Fig. S8.| Microstructure change after aluminum self-ion irradiation (A) irradiation direction and the generation of 1D Al_4C_3 nanorod. (B) Enlargement of white circle Al_4C_3 in (A). The lattice structure: (C) TEM of Al_4C_3 and (E) diffraction pattern [001]. (E) The confirmation of the Al_4C_3 in Al matrix through VASP simulation. The 5-fold division of Al, from (020) to $(\overline{2}\overline{2}0)$, matches the distance of Al_4C_3 from $(\overline{3}10)$ to (210).

Table S1. Experimental parameters of the ion irradiation

Table S2. Composition of Al matrix.

Table S3. VASP simulation of Al_4C_3

Reference

1. Valdés, J. E. *et al.* Energy loss distribution of proton beams at normal incidence on multi-walled carbon nanotubes. *Carbon* **52,** 137–144 (2013).

2. E10 Committee. *Practice for Neutron Radiation Damage Simulation by Charged-Particle Irradiation*. (ASTM International, 2009). at <http://www.astm.org/doiLink.cgi?E521>

3. Kang, J. W., Nguyen, F. T., Lue, N., Dasari, R. R. & Heller, D. A. Measuring Uptake Dynamics of Multiple Identifiable Carbon Nanotube Species via High-Speed Confocal Raman Imaging of Live Cells. *Nano Lett.* **12,** 6170–6174 (2012).

4. E04 Committee. *Test Method for Knoop and Vickers Hardness of Materials*. (ASTM International, 2011). at <http://enterprise.astm.org/filtrexx40.cgi?+REDLINE_PAGES/E384.htm>

5. Muller, D. A., Tzou, Y., Raj, R. & Silcox, J. Mapping sp2 and sp3 states of carbon at sub-nanometre spatial resolution. *Nature* **366,** 725–727 (1993).

6. Berger, S. D., McKenzie, D. R. & Martin, P. J. EELS analysis of vacuum arc-deposited diamond-like films. *Philos. Mag. Lett.* **57,** 285–290 (1988).

Supplementary figures

Fig. S1.

A Control Al   **B** Al/CNTs composite

Crack

5 µm

Fig. S2.

A - Al

500 nm

B – Al/CNT

500 nm

Fig. S3.

Fig. S4.

A Control Al

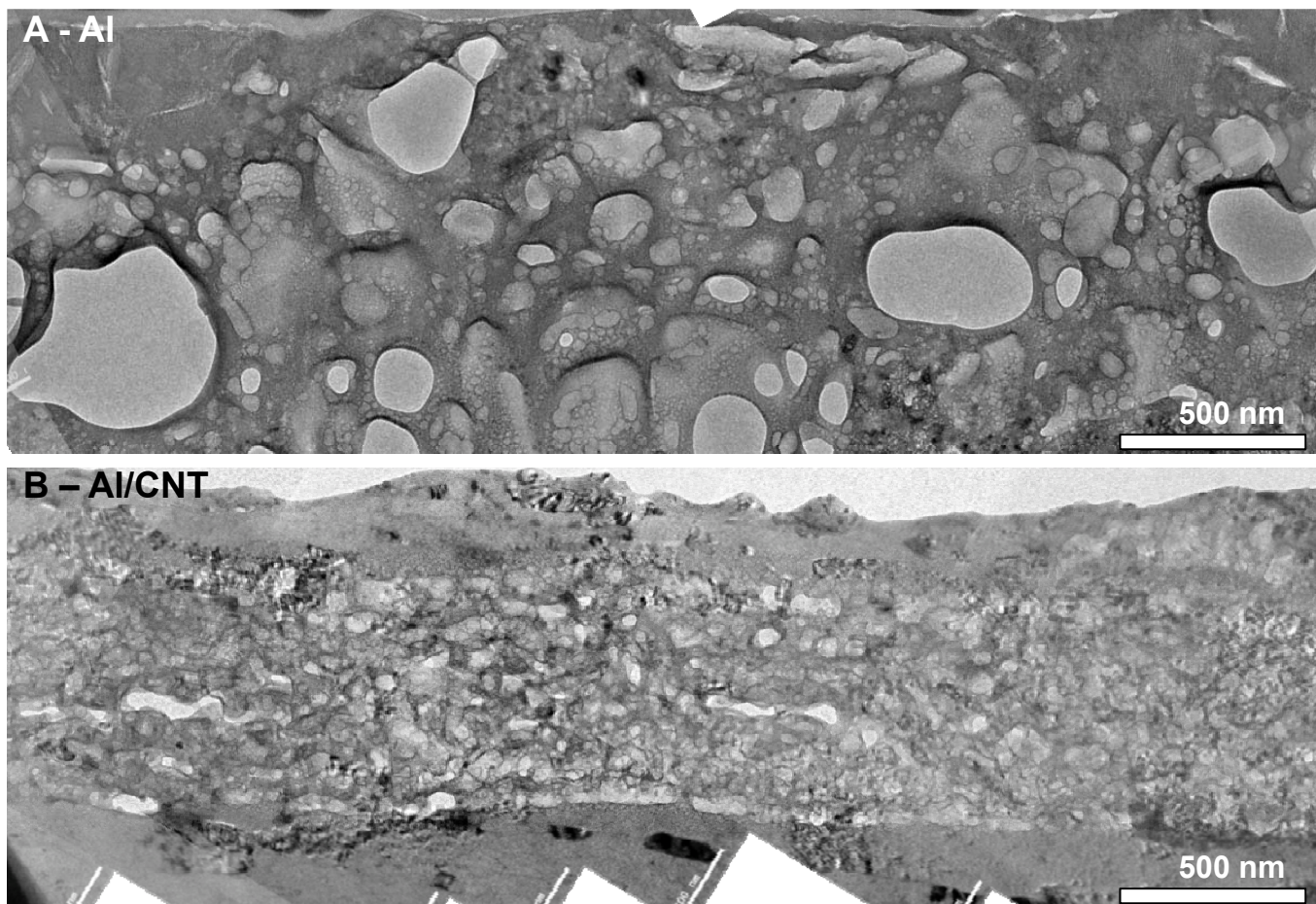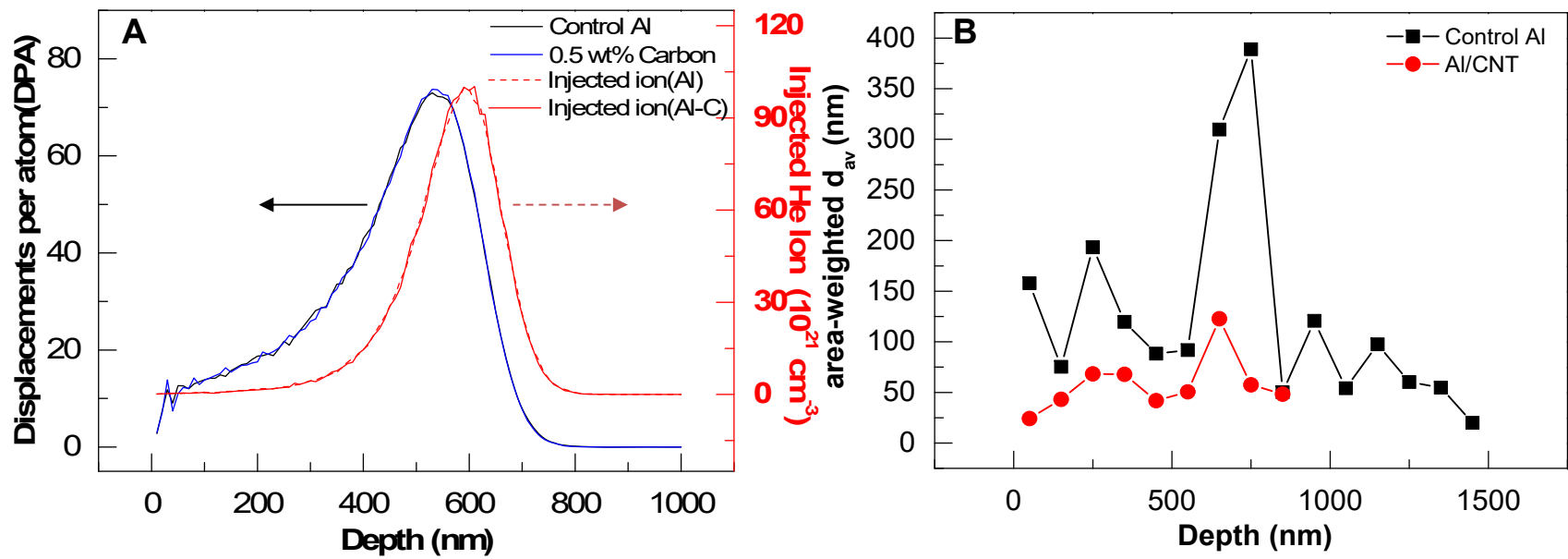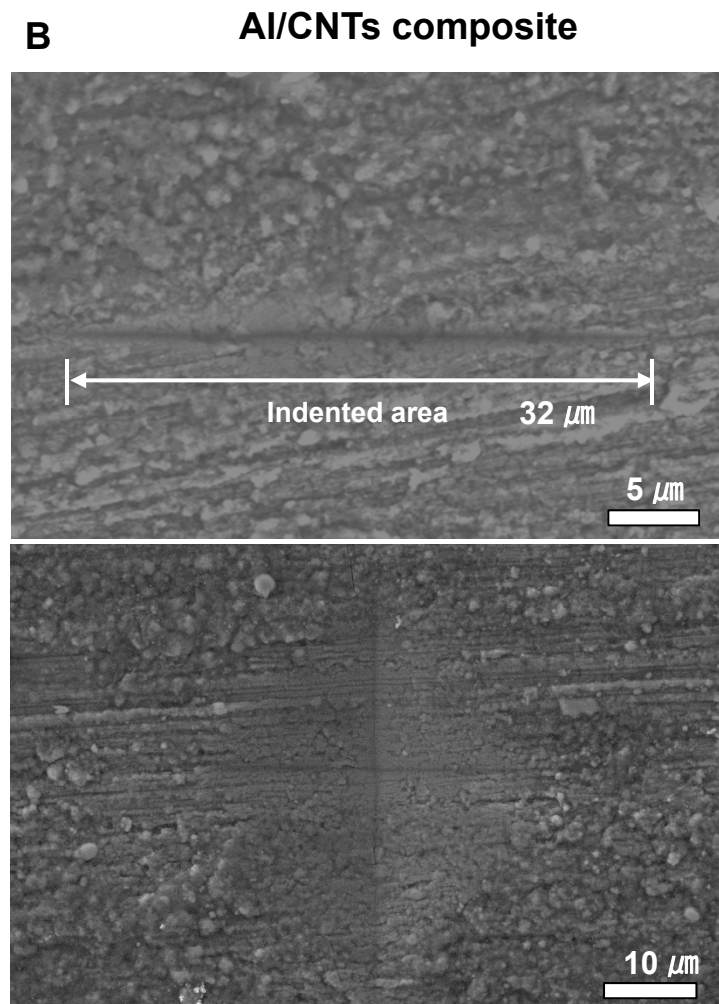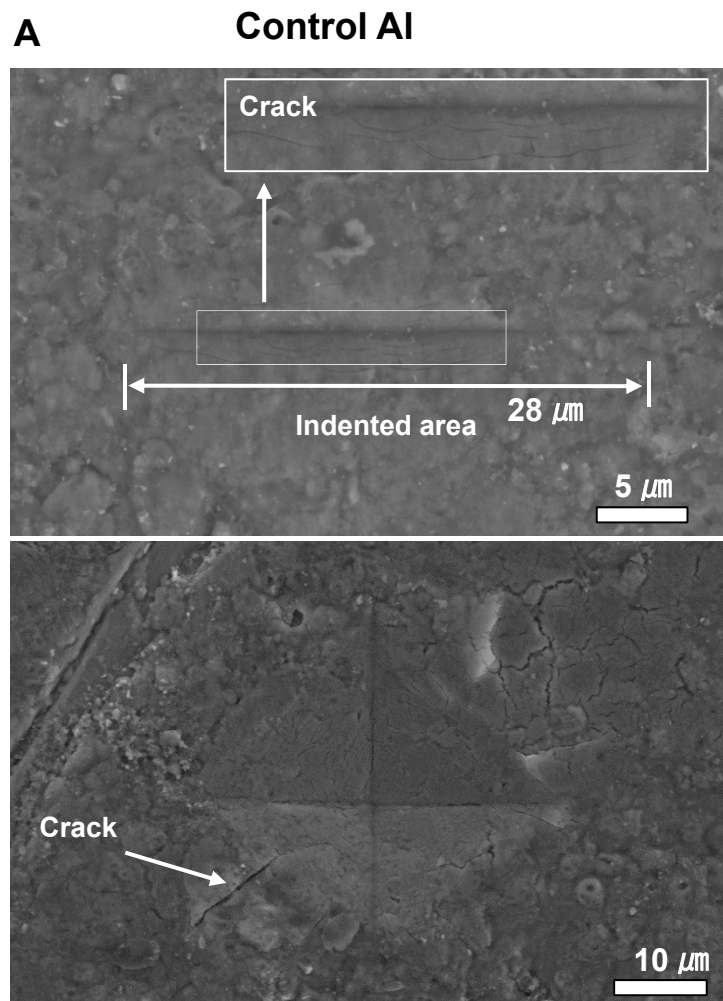**B** Al/CNTs composite

Crack

Indented area 28 μm

5 μm

Crack

10 μm

Indented area 32 μm

5 μm

10 μm
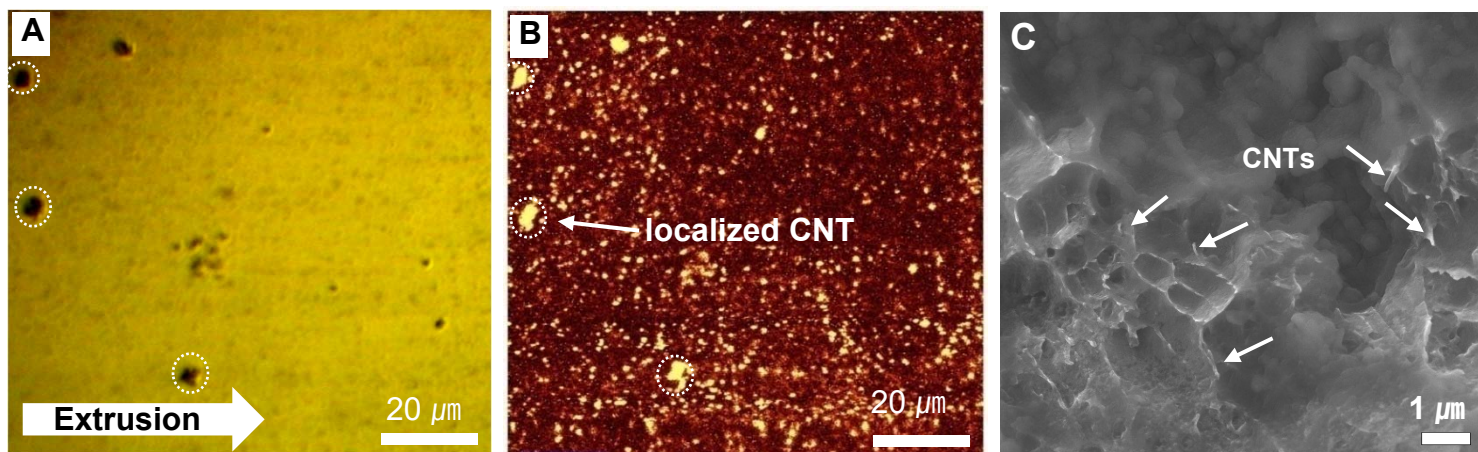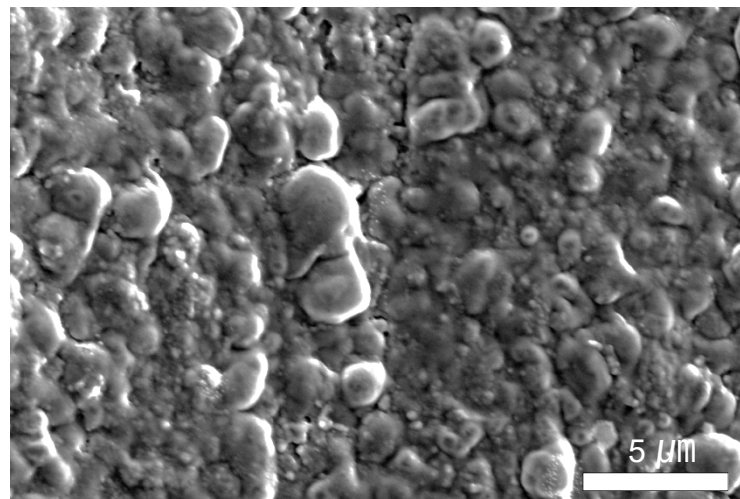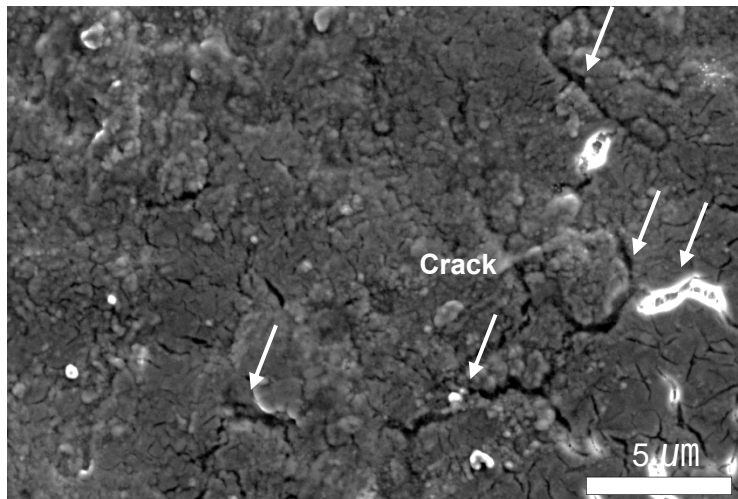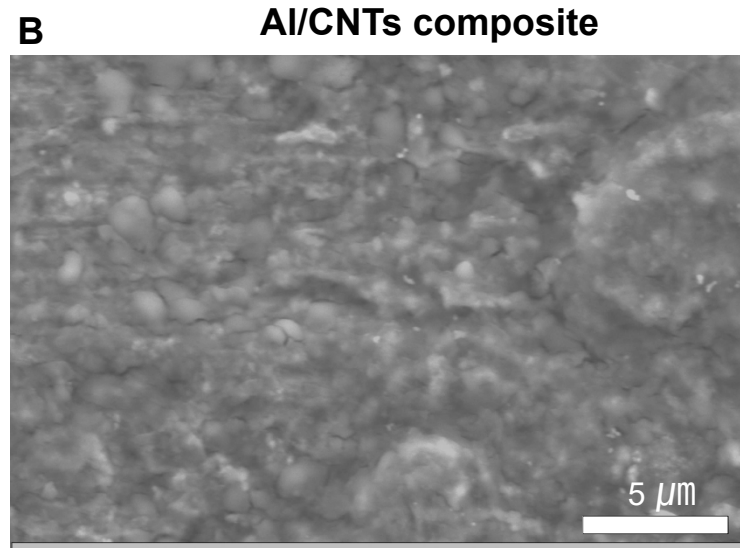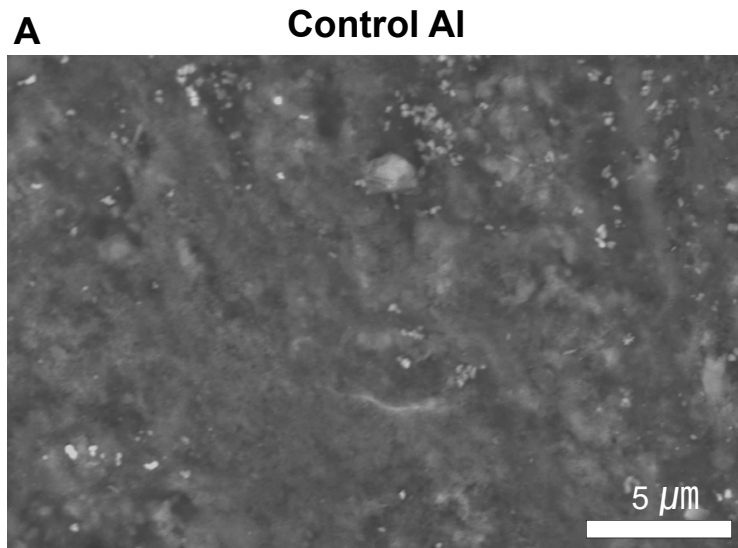
Fig. S5.
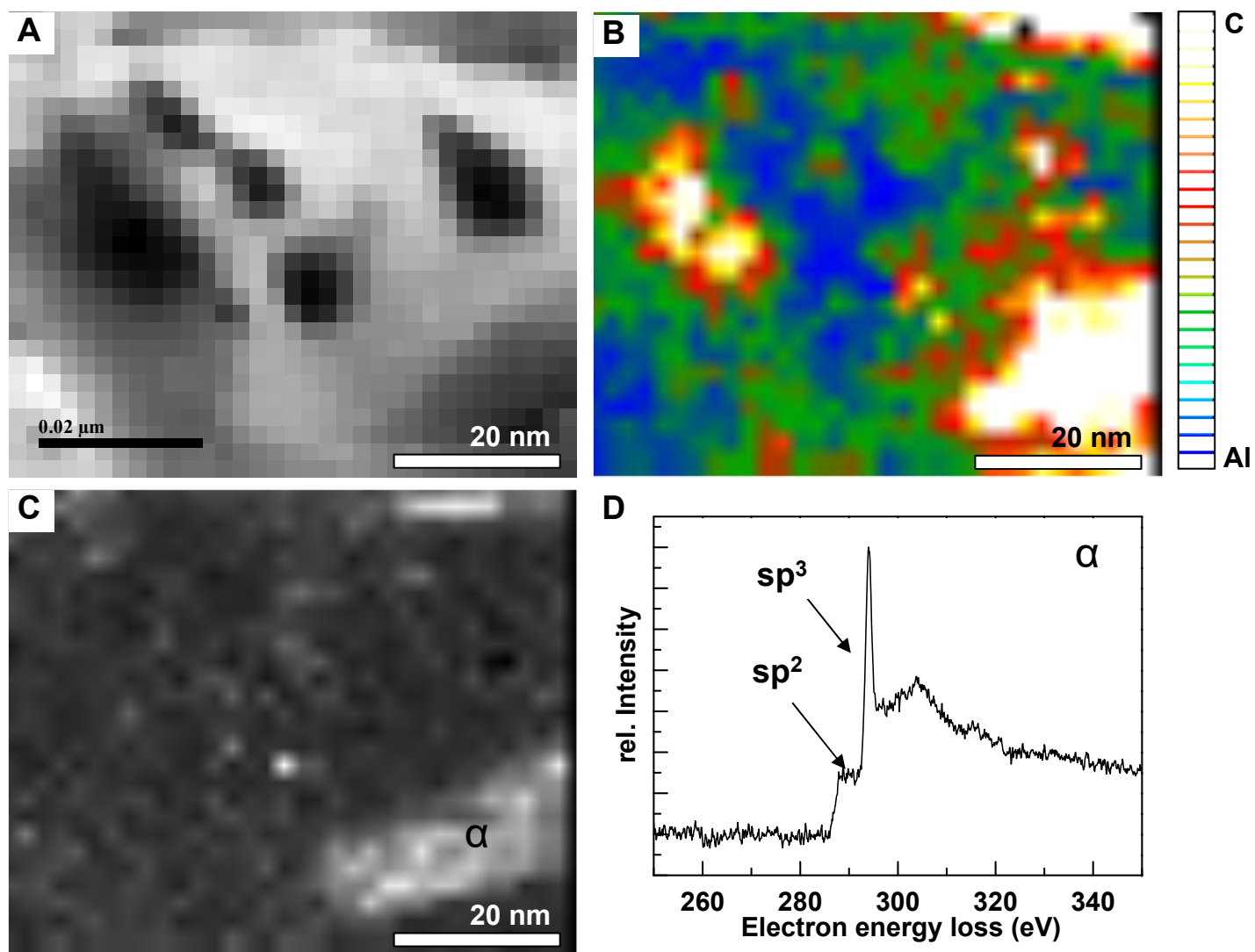
Fig. S6.
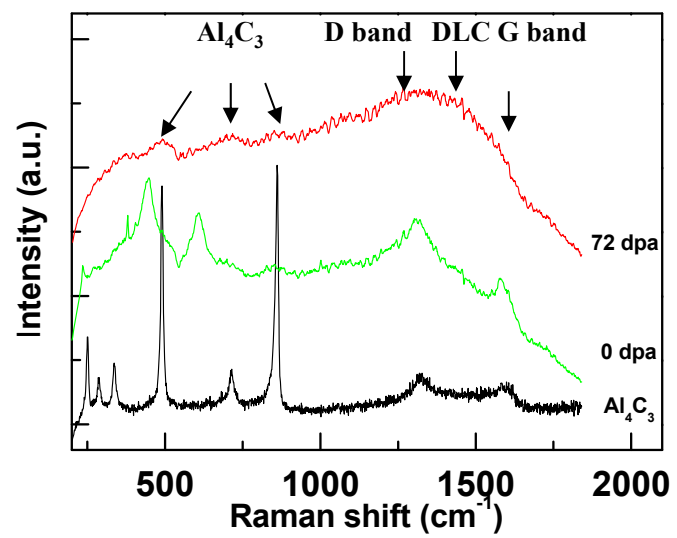
Fig. S7.
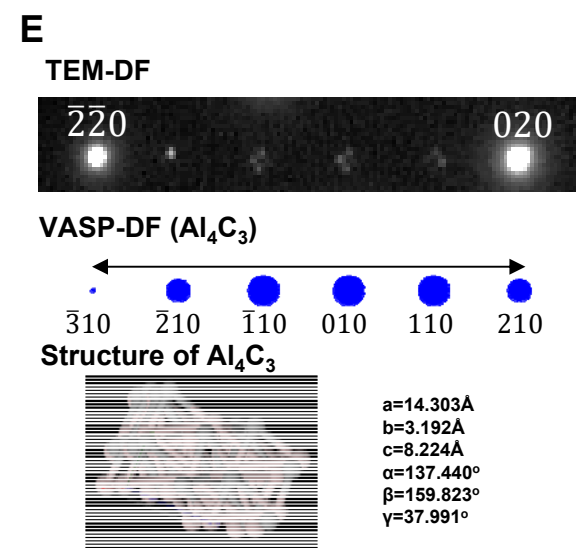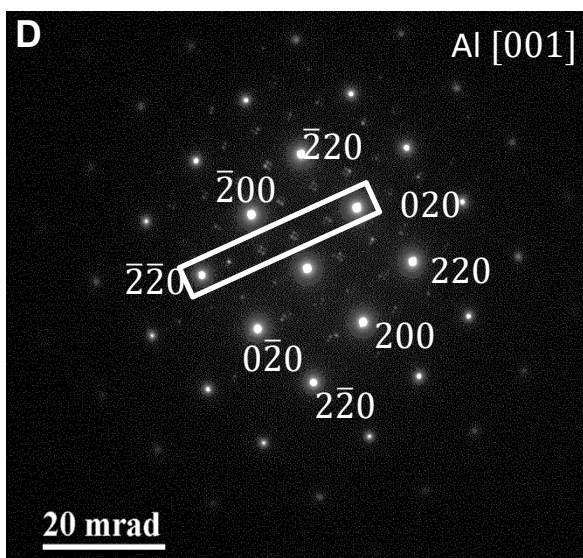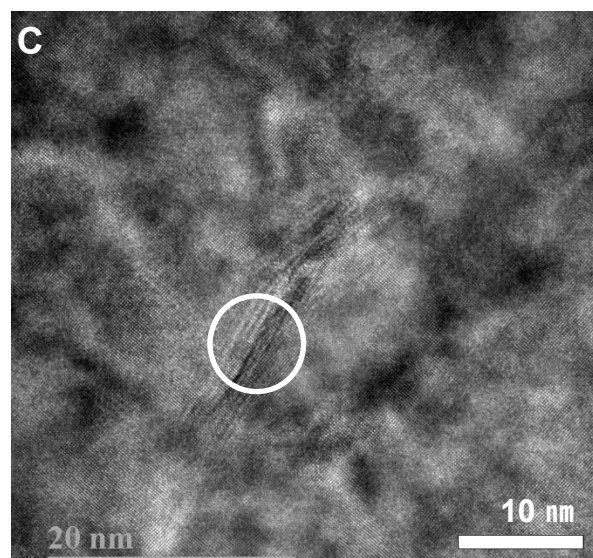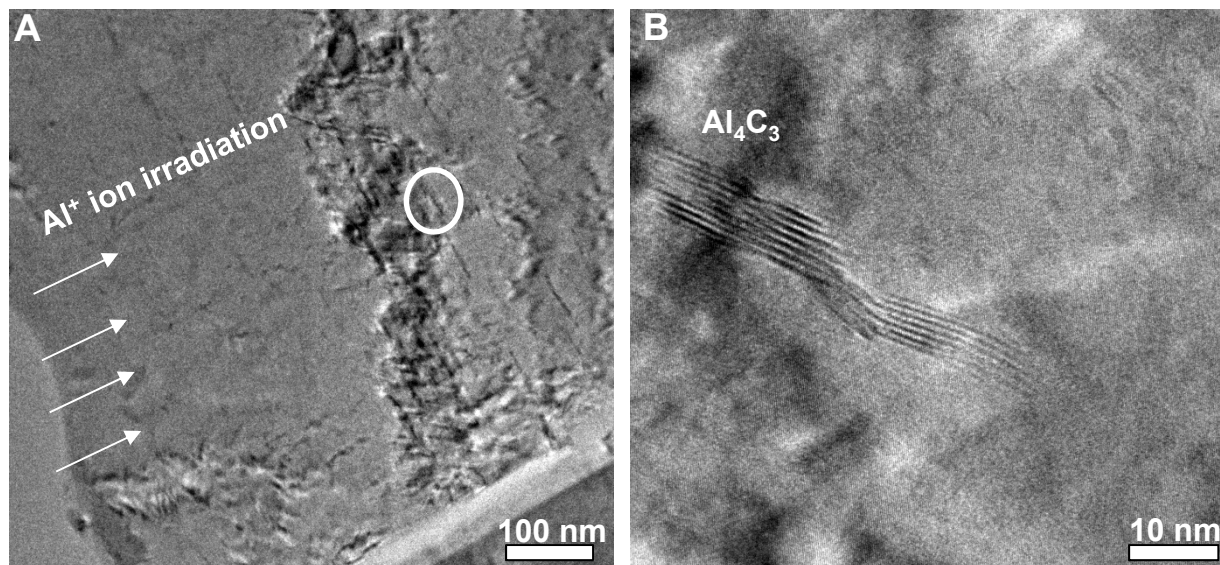
Fig. S8.

Samples	Al	Si	Mg	Fe	Cu	S	Zn	Ga	Cl	Ca	Na	Ni
Al matrix	Balance	0.662564	1.031844	0.150923	1.086861	0.008563	0.067434	0.013915	0.026759	0.048167	0.078138	0.006422

(at%)

Table S1.

Ion species	Samples	Max. DPA	Energy	Beam current	Dose
He$^+$	Control Al/ Al+CNTs 1vol%	3.6	100 keV	400 nA	1E17 cm^{-2}
		16	100 keV	5 uA	5E17 cm^{-2}
		72	100 keV	5 uA	2E18 cm^{-2}
Ar+	Control Al/ Al+CNTs 1vol%	3.6	2MeV	NA	7.5E15 cm^{-2}
		16	2MeV	NA	3.75E16 cm^{-2}
		72	2MeV	NA	1.5E17 cm^{-2}

Note: temperatures are fixed at room temperature

Table S2.

Al_4C_3	Stable	Our nanorod
Kinetic energy cutoff [eV]	520	520
Run type	GGA-PBE	GGA-PBE
K points	Monkhorst-Pack 20x20x20	Monkhorst-Pack 20x20x20
Precision	High	High
E_{tot} [eV]	-43.3295	-40.462108
Fermi energy [eV]	7.29466942	8.75479555
K-S gap [eV]	1.42	0.00

Table S3.